Renewable Energy Based Improved KY Converter with Meta-Heuristic Optimization for EV-Charging Station

K. S. V. V. Prasada Rao[1,*], M. Anitha[2], and V. Srinivasa Rao[3]

ARTICLE INFO

ABSTRACT

Conventional vehicles powered by fossil fuels contribute to air pollution, greenhouse gas emissions, and reliance on finite resources. The urgent need for electric vehicles (EVs) arises as a sustainable alternative, offering reduced emissions, improved air quality, and decreased dependence on fossil fuels for a greener and more sustainable transportation future. As a consequence, this paper proposes an idea of EV charging, wherein these stations is equipped with Renewable Energy Sources (RES) and storage systems. Photovoltaic (PV) system energy output is stored in bi-directional battery. Through the use of a three-phase voltage source inverter (3∅ VSI) and an improved KY converter, the excess energy produced by the panel is fed into the grid. In the absence of solar energy, grid energy is efficiently employed for EV charging. For effectual converter operation optimized controller is essential, of which conventional approaches faces challenges in determining appropriate parameter values, addressing the problem of premature convergence, handling multi-modal optimization problems, and overcoming computational inefficiency in large-scale problems. By resolving these optimization issues Grasshopper Optimized Proportional Integral (PI) controller is utilized in this work, which controls converter operation and ensures a steady supply to Direct Current (DC) connection. Likewise, 3φ VSI connected to grid, is improved by utilizing PI controller. Pulse Width Modulation (PWM) rectifier, which is used when combined with a PI controller in the Wind Energy Conversion System (WECS) with a Doubly Fed Induction Generator (DFIG), facilitates a conversion of Alternating Current (AC) to DC. The simulations are executed in Matlab software and corresponding responses are obtained. The simulated response has 95.2% efficiency and a 1:13 voltage gain as a result.

1. INTRODUCTION

In recent times, the usage of PV power systems is more preferable due to increase in demand on energy and to reduce environmental pollution. Large scale PV power system has been money oriented in many countries due to its durability and schemes provided by government to attain sustainable green energy. It is also suitable in satellite systems, distributed energy generation and transportation. In a solar system connected to grid, optimal power is extracted from PV system and maximum available power is given to the grid [1-2]. PV-interfaced EV concept requires the use of a suitable tracking technique because the output from PV systems is altered by temperature and daylight levels. While operating in particular modes, such as solar panel to grid and vehicle to grid, grid to electric vehicle, PV interfaced EV with grid deliver an oscillatory current to grid with less total harmonic distortion (THD).

The efficiency of the EVs depends on its capacity of charging and discharging [3]. As a result, a step-up gain DC-DC converter is utilized in improving DC voltage received from PV system to achieve need of power equipment. Although the Boost converter cannot regulate input current, it can produce significant gains at high duty ratios. It draws some input current at a high duty cycle from the source, which damages the component elements of the converter [4]. Buck-boost converters can meet step-up or step-down requirements as compared to Boost converters, but their inefficiency prevents them from achieving significant gains. [5].

A voltage from the input can be converted to higher and lower voltage levels in the output by utilizing a typical single switch step down/step up converter, such as Buck converter, Buck-boost converter [6], Cuk [7, 8], Zeta [9] and Single Ended Primary Inductance Converter (SEPIC) [10, 11]. Although Buck boost and Cuk converters are capable of

[1]*Department of Electrical and Electronics Engineering, Annamalai University, Chidambaram, Tamilnadu, India.*
[2]*Department of Electrical Engineering, Annamalai University, Chidambaram, Tamilnadu, India.*
[3]*Department of Electrical and Electronics Engineering, Aditya Engineering College (A), Surampalem, A.P. India.*
Corresponding author: K. S. V. V. Prasada Rao; Email: prasadraoksvv12@gmail.com.

stepping voltages up and down, their efficiency is too low, which offers stress on the component. KY converter has low voltage ripples, speedy transient response to achieve maximum power point and used in photovoltaic systems that operates at Continuous Conduction Mode (CCM) to overcome the complexity due to output ripple waves and voltage transfer gain [12], but it would lead to leakage inductance loss and therefore capacity of a converter is reduced. It is clear that, conventional converters suffer from drawbacks such as lower efficiency, increased power losses, and limited power density. To overcome these limitations, it is essential to adopt an improved converter topology. As a consequence, the proposed work establishes a novel improved KY converter as it offers higher efficiency, reduced losses, and increased power density, resulting in improved overall system performance and energy savings.

A controller strategy is used to balance out the energy obtained from PV system after the converter operation. A PI controller [13] adjusts the control effort based on the error and integral of error, allowing for precise control and steady-state error correction. However, fails in providing faster response and greater performance under variation in input voltage. To tackle the limitations of PI, Fuzzy Logic Controllers (FLC) are introduced [14]. FLC completely depends on human knowledge and rules have to be regularly updated and it cannot recognize machine learning or neural network. To overcome these drawbacks, metaheuristic optimization algorithms are opted for an optimal tuning of PI controller. Genetic Algorithm (GA) is an algorithm based on population, which utilizes the concept of biological evolution and survival of fittest. The main operators of GA are selection, crossover, and mutation [15] so that the process of iteration is very slow, difficult to understand and debug.

Grey Wolf Optimization (GWO) Algorithm takes into account leadership structure and hunting habits of the grey wolves. Although its implementation with fewer parameters is simple, its performance is affected by truncated solution accuracy and slow convergence speed [16]. To achieve the best result, the Particle Swarm Optimization (PSO) method makes use of individual cooperation and information exchange. Each particle changes its velocity and position by keeping track of both local and global extreme values during each iteration [17], but it has low convergence speed in its iteration process. Whale Optimization Algorithm (WOA) is a meta-heuristic optimization algorithm that models the humpback whales' foraging behavior. However, it has difficulty determining the optimal solution to high-dimensional, challenging optimization problems [18]. In this research, we apply a metaheuristic optimization algorithm, Grasshopper Optimization Algorithm (GOA), to foraging and swarming behavior of grasshoppers in nature. GOA can be used in many different fields, including wind energy, distributed generation, load frequency management, feature selection, and scheduling [19-20].

Mechanical systems, electric generators, integration with power systems, aerodynamic design, Pressure to Electric Converter, and control theory have all improved in the wind energy sector during the past ten years. The wind turbine (WT), which is coupled to the DFIG and has low converter ratings with effective power collection due to variable speed operations, is one of the various WECS technology types that is most used. Most existing wind turbines utilize the DFIG, which provides about 50% of all installations. DFIG offers high torque and reduction in size since it makes effective use of the rotor core. [21-22].

A 3ϕVSI transmits the power generated by DC-DC converter to the grid [23]. It gives a grid an AC output with a lower THD value at a given frequency. A superior AC output is produced and supplied into the grid thanks to the usage of PI controllers, which compare real power and reference power to govern inverter operation [24].

A PV integrated grid system with improved KY converter is examined in this proposed work, in which converter is controlled by means of PI controller assisted with GOA. The grid is supplied with the retained DC voltage through a 3ϕ VSI. PI controller has been utilized to regulate the VSI, which is used for efficient grid synchronization and improved reactive power adjustment. LC filter [25] is used to suppress a harmonics obtained from a system, which in turn improves the system stability [26]. The contributions of study are as follows,

- Development of an efficient microgrid powered by renewable energy sources (RESs) aimed at significantly reducing the reliance on fossil fuels and combating the pressing issue of global warming.

- Reducing the use of fossil fuels and battling global warming by utilizing PV and WECS as the primary energy sources.

- Maintaining a constant voltage supply by using an improved KY converter with GOA assisted PI controller.

- Using a PI controller to stabilize a WECS based on DFIG output.

- Providing grid synchronization with conventional PI controller thereby enabling uninterrupted power supply for EV charging.

Using MATLAB software, the voltage stability is practically confirmed.

2. PROPOSED SYSTEM DESCRIPTION

By storing wind power at night and solar electricity during the day, EV may be charged from renewable energy sources, which in turn promotes the growth of renewable energy and lowers greenhouse gas emissions. PV integrated to grid with improved KY converter is proposed with the GOA based PI controller, which is synchronized with the grid through a 3ϕVSI control scheme as presented in Fig. 1.
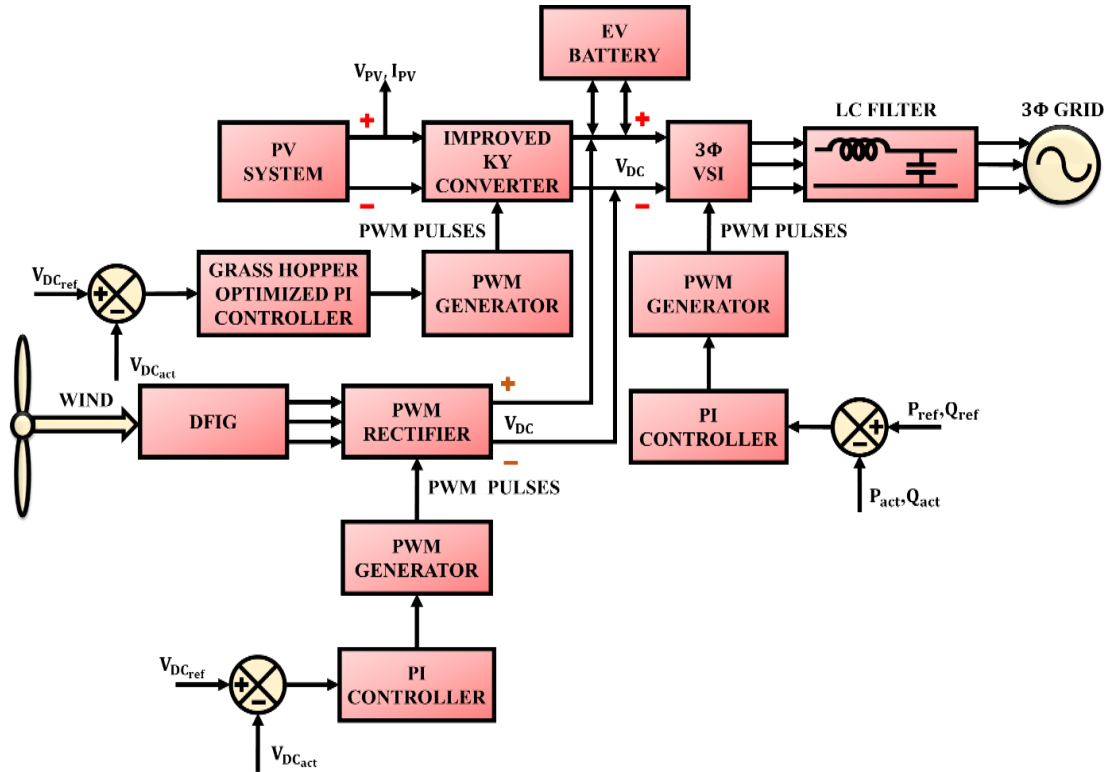
Fig. 1. EV Charging Station Modelling.

Due to solar irradiation and temperature changes, the output from PV system is influenced, that provides a low voltage. Hence, there is a need of converter to increase DC voltage to higher value. Improved KY converter is employed in this proposed paper. A GOA based PI controller is employed in this proposed system to optimize the parameters of PI, comparing $V_{Dc_{ref}}$ with $V_{DC_{act}}$ through which the PWM pulses are generated to the Improved KY converter. The wind energy fed into DFIG is supplied to PWM rectifier and the obtained value is fed to grid through 3ϕ VSI, which leads to conversion of DC-AC. To achieve synchronization the supply from inverter is effectively controlled using PI Controller by analogizing $P_{ref}Q_{ref}$ with $P_{act}Q_{act}$. The compared signal is given to PWM generator which widen the amplitude and provides optimal supply to gird. Thus, grid synchronization is achieved.

3. PROPOSED SYSTEM MODELLING

3.1. Modelling of PV cell

Sunlight is directly converted into electricity by a PV system, a type of RES. It involves solar panels made up of PV cells that generate electrical energy when exposed to sunlight. These cells are typically made of semiconducting materials, such as silicon, which produce an electric current when photons from sunlight strike them. In this study, the PV panel is constructed using a single diode circuit type PV

array, which has the advantage of being convenient to build and assess PV performance.

To model the PV array with a single diode circuit, four parameters are needed. Those are short circuit current (I_{sc}), series resistance (R_s), open circuit voltage(V_{OC}) and shunt resistance. The diode (D) of the model PV cell is linked across the current source (I_{pv}). Fig. 2 indicates the PV parallel circuit.
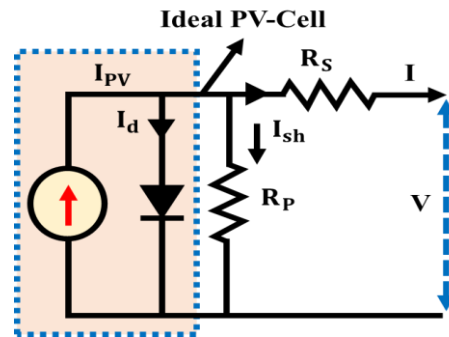
Fig. 2. Equivalent circuit of PV cell.

A PV cell's output current is given by,

$$I = I_{ph}N_{pp} - I_0 N_{pp}\left(exp\left(\frac{V+IR_S(N_{SS}/N_{pp})}{a*V_1*N_{SS}}\right)-1\right) - \frac{V+IR_S(N_{SS}/N_{pp})}{R*(N_{SS}/N_{pp})} \quad (1)$$

where, I_o is reverse saturation current and I_{ph} is photon current. Power rating of PV panel is preserved by improving parallel (N_{pp}) and series (N_{ss}) connection of cells.

$$I_{ph} = (I_{ph_{STC}} + k_1 \Delta T) * G/G_{STC} \qquad (2)$$

From Eq. (2), change in air temperature and irradiation conditions has a direct relationship with the variation in photocurrent. Eq. (3) contains the reverse saturation current for a diode, and it hinges on the operation temperature and material properties of the diode production process.

$$I_o = \frac{I_{SC_{STC}} + k_i \Delta T}{\exp\left(\frac{V_{OC_{STC}} + K_v \Delta T}{\left[\frac{a}{p}\right] V_t}\right) - 1} \qquad (3)$$

The equation utilizes the temperature coefficients, voltage, and current values to calculate the current output at the given operating temperature (ΔT). It considers the impact of temperature on the performance of PV module by adjusting the current and voltage values accordingly [27].

However, converter is essential, which is responsible for enhancing the voltage generated by the solar panels that is suitable for the use of electrical grid and most electrical appliances.

3.2. Improved KY converter

KY converter boosts the PV voltage and offers rapid transient response when compared to conventional Boost converter. However, a gain of KY converter can be enhanced with an adopting of improved configuration. The improved KY converter has a minimal output voltage ripple and an input voltage is less compared to output voltage. By virtue of synchronous rectification, the current from the converter is steady and controllable.

The improved KY converter consists of power switch S along with diodes D_1, D_2, capacitors C_1, C_2, output capacitor C_o which is used to provide constant voltage across itself, and two inductors L_1 , L_2. Number of switches is reduced in an improved KY converter. In the circuit shown in Fig. 3, an input voltage and output voltage are indicated by V_{in} and V_o and duty cycle is represented as D. Voltage across capacitors C_1, C_2, C_o are V_{C1}, V_{C2} and V_{CO}, and voltage across the diodes D_1, D_2 are V_{D1} , V_{D2} and voltage across inductor L_1 is denoted by V_{L1} respectively.

Continuous conduction mode is used to operate the upgraded KY converter. To make the analysis easier, the following standards are considered:

1) The rating of input voltage V_{in} is constant.

2) As the voltages across all capacitors are consistent for one switching period, they are all large enough.

3) All elements are normal and parasitic components are eliminated.
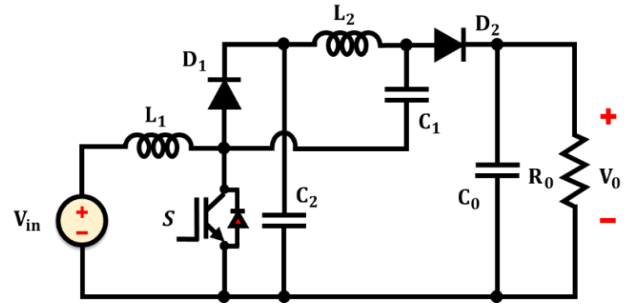
Fig. 3. Improved KY Converter.

3.2.1. Continuous Conduction Mode operation

The discussion that follows is limited to the proposed DC-DC converter's CCM operation during one switching phase. It has two operating modes. Fig. 3 displays the equivalent circuit, and Fig. 5 presents the converter waveform operated in CCM. A converter operation in CCM is given in the following and the operating modes are presented in Fig. 4.

(a)

(b)
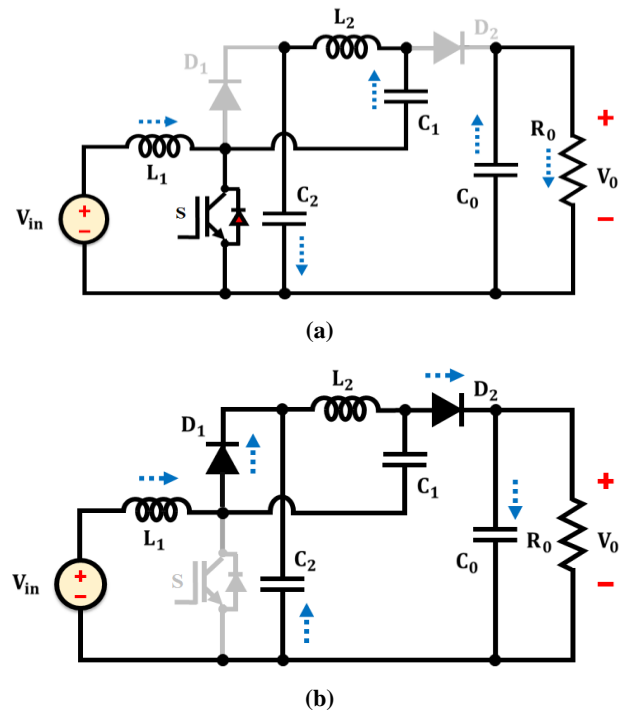
Fig. 4. Operation at CCM (a) Mode 1 (b) Mode 2.

Mode 1[t_0, t_1]: Switch S is first switched on in this mode, and the diodes are in the off (blocked) condition. Current of inductors are linearly increased with the input voltage (V_{in}). During t_0 and t_1, capacitor C_1 is charged and capacitors C_2, C_0 are discharged and energy from the output capacitor is transmitted to the output load. A first mode ends when the power switch turns off at t=t_1. During the first mode shown in Fig. 4(a), voltage across an inductors L_1 and L_2 are achieved, as follows;

$$V_{L1(mode\ 1)} = V_{in} \qquad (4)$$

$$V_{L2(mode\ 1)}=V_{C2}-V_{C1} \tag{5}$$

Mode 2[t_1,t_2]: In second mode, switch S is turned off, the diodes D_1 and D_2 starts conducting as shown in Fig. 4(b). A stored energy is decreased, and their current is decreased to their minimal value. The capacitor C_2 is charged at this transition time. This operation finishes when the switch S is turned on for the next switching period.

The voltage across inductors L_1,L_2 are as follows.

$$V_{L1(mode\ 2)}=V_{in}-V_{C2} \tag{6}$$

$$V_{L2(mode2)}= -V_{C1} \tag{7}$$

The converter's voltage gain is obtained by,

$$M=\frac{(1+D)}{(1-D)} \tag{8}$$
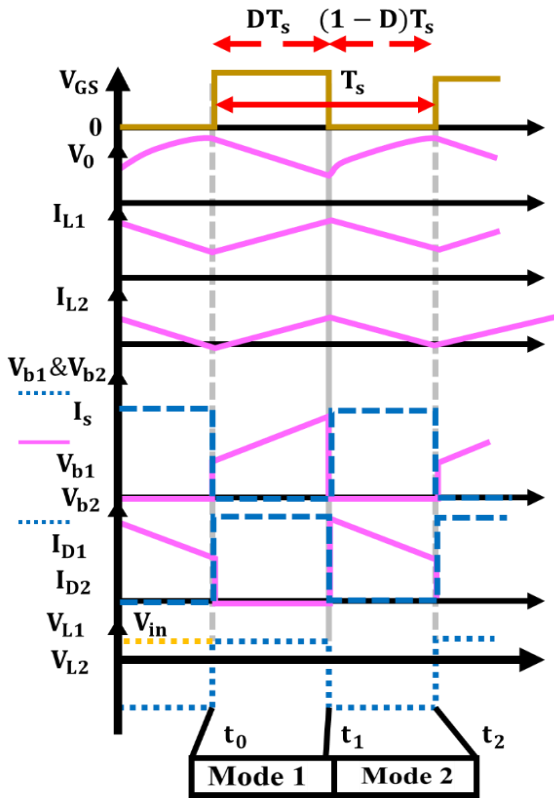
Fig. 5. Waveform of converter operation in CCM.

The output voltage is larger than input voltage and it provides quick transient load response, smaller voltage ripple and its accuracy is high. Additionally, this converter is easy to design, and the controlling method is simple, so it is applicable in industrial aspects. The optimized control methodology of the converter used in this work is explained as follows.

3.3. GOA based PI controller

A PI controller regulates the operation of a converter, which helps to produce control signals for the converter to work properly. However, gain parameters of conventional PI

controller are selected by trial-and-error method which does not guarantee the generation of accurate outputs. Hence optimization algorithms are adopted to decide the PI controller parameters for the generation of optimal outputs. The swarming behavior of grasshoppers in nature serves as inspiration for the GOA, a nature-inspired metaheuristic optimization algorithm. GOA is a present-day multi-layered systematic method designed on the grasshopper's life cycle, which comprises three stages such as egg, nymph and adult that goes under a transformation process known as metamorphosis. As sliding cylinders, grasshoppers migrate from egg to nymph and when they wander from nymph to metamorphosis, they disrupt the growth of crops. This algorithm is arithmetically designed to form a functional optimization technique called GOA. It has two functions: it searches for members at first during the exploration phase, and later it moves close by during the exploitation phase. This process guarantees that the goal is executed reasonably [28].

The expression for the behavior of 'Grasshoppers' in flock:

$$X_m = r_1 S_m + r_2 G_m + r_3 A_m \tag{9}$$

where, S_m is the correlation, A_m is the wind in abeyance, and X_m is the location of mth Grasshopper and G_m is the gravitational strength on m^{th} Grasshopper. The renewed equation for arbitrary nature is obtained by,

$$X_m = r_1 S_m + r_2 G_m + r_3 A_m \tag{10}$$

where, r_1, r_2 and r_3 are arbitrary coefficients. The reputation and attraction forces, which connect a grasshopper with its next place, are two adjacent forces among grasshoppers that serve as an example of the social interaction amongst grasshoppers in nature. The continuous force leads them to examine the suitable space, while the attraction force permits grasshoppers to quarry the beneficial area (local search) (global search). Comfort zone refers to the region where these forces are equal, and the target position is still to be tested.

As a result, the grasshopper's location has the best fitness because it will be targeted by the closest one. The grasshoppers keep moving in the target's main direction to achieve balance between local and global search to approach the target. The comfort zone gradually disappears as grasshopper places are renewed. At last, the grasshopper reaches its destination.

The steps to be followed in GOA are listed below.

1. **Initialization:** $c_{max}, c_{min}, t_{max}$ values are being fixed to initiate the algorithm.

2. **Assessment and initial population:** Selection of the inhabitants is initially done arbitrarily and based on the target; the solutions are examined.

3. **The ideal solution description:** Based on how valuable it is, the best answer is chosen.

4. Changing the reducing factor: The value of c is changed for reducing the controllable situation.

5. Maintaining the distance among the solution: Eq. (9) has the control to split up the repulsion, the attraction zones and the comfort.

6. Renovating the solution: Renewal of the solution depends upon the distance between it and alternative solutions can be obtained by Eq. (10).

7. Boundary violation with the solution: The solution will rest in its domain if it enters the border. For all population-based, local, and global solutions, the above three processes are replayed.

8. Ending procedure: The general process is continued till the maximum number of iterations or t_{max}, has been attained.

9. The complete answer is then presented.

This procedure is explained as a flowchart in Fig. 6.
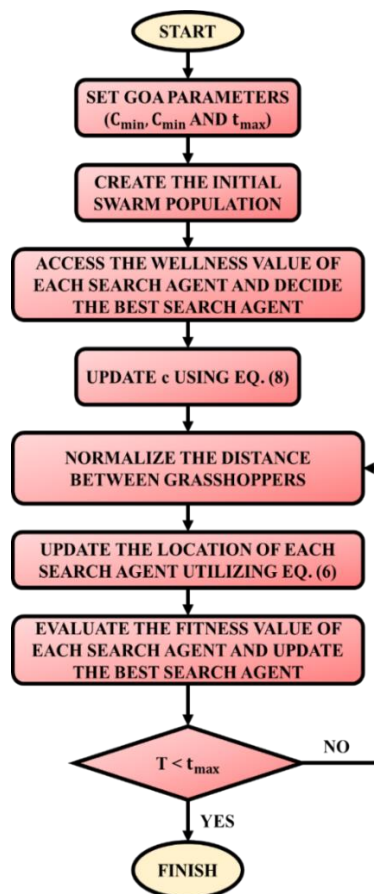
Fig. 6. Flowchart of GOA.

The arithmetic depression of the process is explained by taking the d-dimensional location of the ith grasshopper in the swarm, G is the grasshopper in the swarm.

$$\sum_{\substack{j=1 \\ j \neq i}}^{G} c \frac{ub_d - lb_d}{2} s(|x_j^d(t) - x_i^d(t)|) \frac{x_j(t) - x_i(t)}{d_{ij}}) + \widehat{T_d} \quad (11)$$

$$s(r) = f \exp\left(\frac{-r}{l}\right) - \exp(-r) \quad (12)$$

The value of c is consistently fixed between c_{max} and c_{min}, and the usage of high rate of c endup with more utilization.

$$c(t) = c_{max} - t \frac{c_{max} - c_{min}}{t_{max}} \quad (13)$$

The optimal representation of the GOA is given in Table 1.

Table 1. Features of optimal GOA

Number of search agents	50
c_{max}	1
c_{min}	0.00004
t_{max}	50
f	0.5
l	1.5
ub_d	10
lb_d	-10

In GOA, the location of a single grasshopper is renovated with its location of other grasshopper, actual position and globally best position. Hence, GOA motivates all agents of search to get involved in optimization process, which gives rise to high performance of the search. The values of k_p and k_i used in GOA based PI controller are 4.5 and 2.1 respectively, which provides less steady-state error and better damping behavior. GOA provides better performance in symmetrical (balanced) and asymmetrical (unbalanced) situations, making it suitable for optimization problems with both equal and unequal constraints and variables. Since energy is required during long travel, charging of the batteries is required and so a DFIG based WECS is modelled for the continuous usage of the vehicle.

3.4. Modelling of DFIG based WECS

DFIG as seen in Fig. 7, is an asynchronous generator wound with rotor in which the grid is connected to stator and rotor through a converter. Due to low quality of the converters connecting the grid to DFIG, the wide speed operational range and the capability of adjusting active and reactive powers, DFIGs now take over the market for WECS.

When compared to fixed speed wind turbines, the DFIG-based WECS also offers greater energy absorption, quality in power, and less internal forces on the motor. To reduce the complexity, the dynamic model written in arbitrary rotating frame dq was adopted.
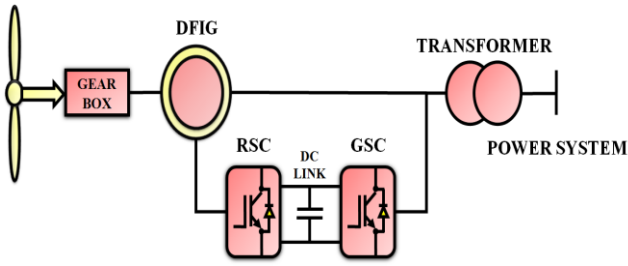
Fig. 7. DFIG based WECS.

$$\begin{cases} v_{ds} = R_s i_{ds} + \frac{d}{dt}\phi_{ds} - \omega_s\phi_{qs} \\ v_{qs=} R_s i_{qs} + \frac{d}{dt}\phi_{ds} + \omega_s\phi_{ds} \\ v_{dr=} R_r i_{dr} + \frac{d}{dt}\phi_{dr} - \omega_r\phi_{qr} \\ v_{qs} = R_r i_{qr} + \frac{d}{dt}\phi_{qr} + \omega_r\phi_{dr} \end{cases} \quad (14)$$

Equation (14) indicates the voltage equation for Stator and Rotor.

Where r and s denotes the rotor and the stator indices respectively, d and q are the synchronous reference frame components. ω, ϕ, i and v, denotes the electrical frequency, the flux, the current and voltage respectively. R is the resistance.

$$\begin{cases} \phi_{ds} = L_s i_{ds} + M i_{dr} \\ \phi_{qs} = L_s i_{qs} + M i_{qr} \\ \phi_{dr} = L_r i_{dr} + M i_{ds} \\ \phi_{qr} = L_r i_{qr} + M i_{qs} \end{cases} \quad (15)$$

Equation (15) indicates the flux equation for Stator and Rotor, where Mutual inductance is M and Inductance is L

The equation for DFIG-based WECS can be written mechanically as,

$$\text{J}\frac{d\Omega}{dt} = T_a - T_{em} - f\Omega \quad (16)$$

where, T_{em} is the generator electromagnetic torque, Ω is the DFIG speed, J turbine total inertia, and f is the damping coefficient.

An electromagnetic torque for DFIG is known as:

$$T_{em} = p\frac{M}{L_s}\left(\phi_{qs}i_{dr} - \phi_{ds}i_{qr}\right) \quad (17)$$

Where number of the pole pairs of DFIG is p.

$$\begin{cases} P_S = \frac{3}{2}(v_{ds}i_{ds} + v_{qs}i_{qs} \\ Q_S = \frac{3}{2}(v_{qs}i_{ds} - v_{ds}v_{ds}i_{qs)} \end{cases} \quad (18)$$

Equation (18) indicates the expressions of active and reactive power for stator side [29]. The output obtained from DFIG may oscillate at its normal operation because of blowing wind. If it is not maintained regularly, it affects the quality of the energy, frequency, voltage and stability of a power system. To have a uninterrupted supply to the grid, synchronization of the voltage is required which is obtained

from the DC voltage applied to the PI controller and then PWM pulse is generated, then the energy produced is supplied to the battery and the grid for working of the system.
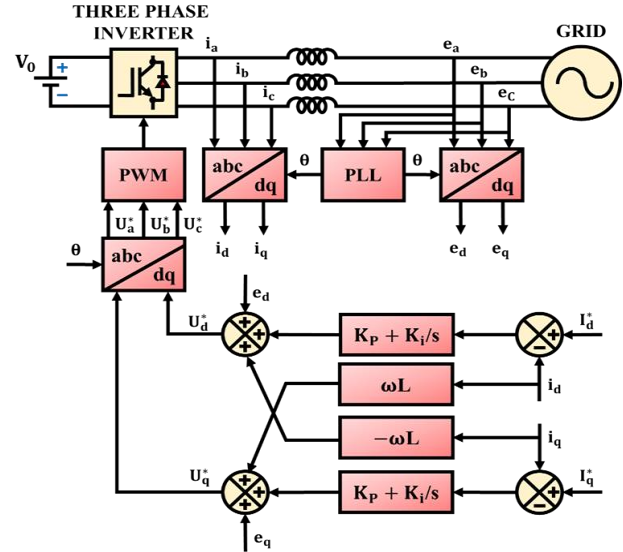
Fig. 8. Configuration of grid connected 3ϕ VSI.

3.5. Grid Voltage Synchronization

Grid synchronization is the process of aligning frequency, voltage, and phase of a distributed energy resource system with the existing electrical grid to enable seamless integration and safe operation. It is necessary to ensure reliable and efficient power transfer, prevent disruptions, and maintain grid stability. For grid voltage synchronization, a PI controller based current control method used is explained in Fig. 8. This method is less susceptible to fluctuations in grid power and responds more quickly. PI controller aims to reduce inaccuracy when evaluating an actual VSI output current to a desired reference current.

The proportional term in control system is formed by combining error and proportional gain, effectively reduces the overall error. By incorporating an integral term attained through multiplying error by an integral gain, steady-state error is eliminated. The proposed grid voltage synchronization method ensures improved steady-state response, while also minimizing harmonics and maintaining active and reactive power components using PWM techniques.

4. RESULTS AND DISCUSSION

An improved KY converter strategy for raising PV system productivity is presented in this paper. As a result, the PWM generator and GOA-based PI controller work together to provide the DC link with regulated voltage. The 3ϕ VSI maintains swapping operations over PI controller. In

Matlab, the final system approach is carried out, and simulation results are acquired. Table 2 shows a description of the proposed system's parameters.

Temperature and radiation waveforms of the PV system are shown in Fig. 9(a). From 0 to 0.1s, the temperature waveform displays a persistent 20°C temperature. Then it reaches a temperature of about 35°C at 0.1s, and it is retained to be constant throughout the system. The voltage produced by the PV system increases because of the abrupt rise in temperature.

Table 2. Parameters Description

Parameters	Descriptions
Solar PV system	
Peak Power	10KW, 10 panels
Series Connected Solar PV Cells	36
Short Circuit Current	8.3 A
Open Circuit Voltage	12V
Battery	100 Ah, 10V
Improved KY Converter	
L_1,L_2	$2*(350\mu H - 6A)$
C_1,C_2	$47\mu F$
Switching Frequency	10KHz

4.1 At varying temperature and irradiation
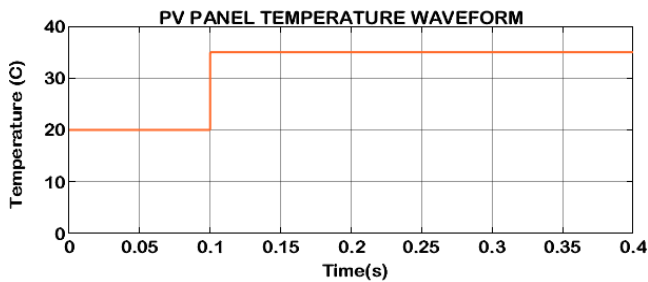
(a)
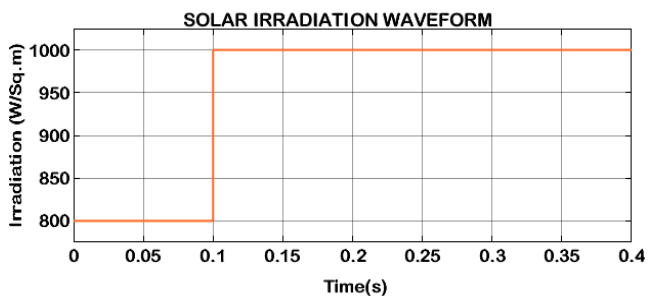
(b)

Fig. 9. Solar Panel Parameters at varying condition (a) Temperature Waveform (b) Solar Irradiation Waveform.

In due course, the solar irradiation waveform, Fig. 9(b) shows that, from 0 to 0.1s there is a stable irradiation. At 0.1s, there is sudden rise in the irradiation of 1000W/sq-m, after that it is maintained to be constant throughout the system.
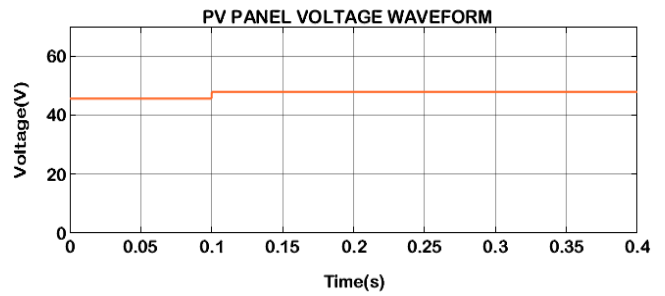
(a)
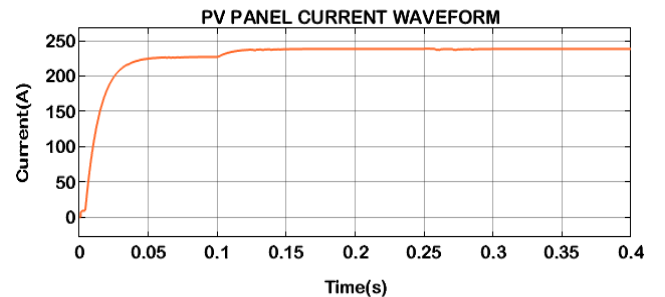
(b)

Fig. 10. PV Panel output at varying condition (a) Voltage waveform (b) Current waveform.

An output current and voltage waveform of the PV panel is shown in Fig. 10, in which, the voltage waveform indicated in Fig. 10(a) has a constant voltage of 42V and at 0.1s there is slight variation in voltage and it is constantly maintained at the voltage of 48V. Fig. 10(b) indicates the current output of PV panel, in which it is gradually raised initially and becomes constant at 240A after 0.1s.

Fig. 11 depicts the waveform for an output voltage and current waveforms produced by proposed converter. An input to the converter is obtained from the PV panel. The first waveform, Fig. 11(a) represents an output voltage waveform of converter, at 0.01s there is a disruption in voltage, and it becomes stable after 0.05s and a constant voltage of 620V is maintained after 0.3s. Likewise, Fig. 11(b) denotes the converter's output current. Initially, the current is disrupted and there is gradual rise of current at 0.03s, then the current is maintained constant at 13A.

(a)

(b)
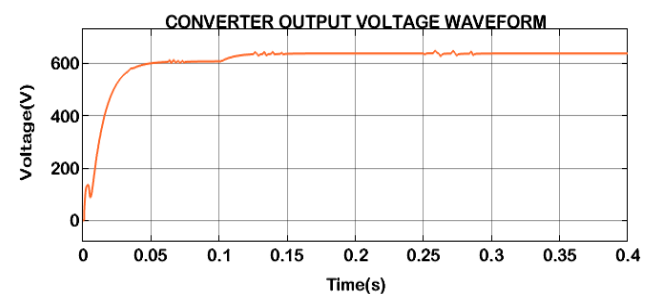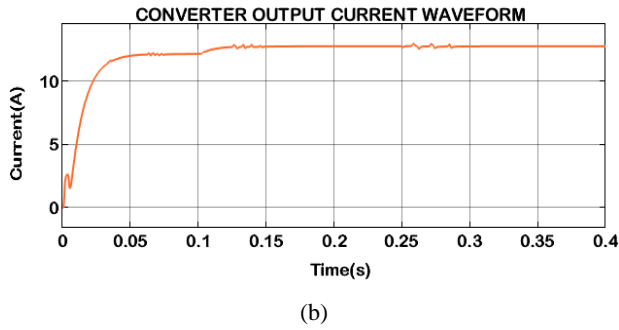
Fig. 11. Converter waveforms at varying condition (a) Voltage (b) Current.

4.2 At constant temperature and irradiation

(a)

(b)
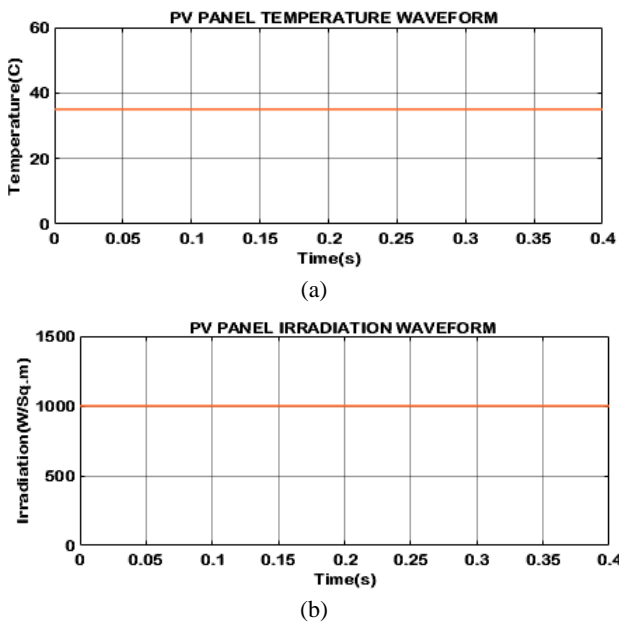
Fig. 12. Solar Panel Parameters at constant condition (a) Temperature Waveform (b) Solar Irradiation Waveform

Fig. 12 represents the output waveforms for solar irradiation and temperature at constant condition. A constant temperature of 35°C is maintained throughout time period as shown in Fig. 12 (a) whereas a solar irradiation of 1000W/sq-m is indicated in Fig. 12 (b).

(a)

(b)
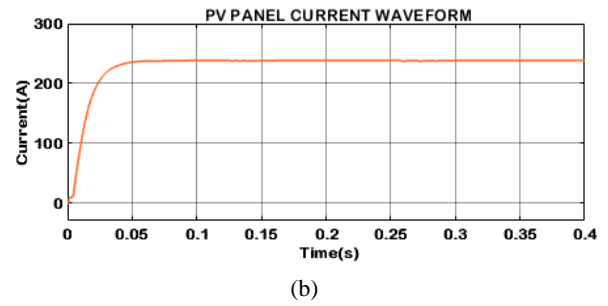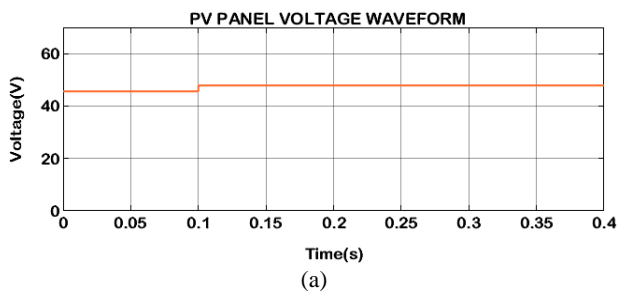
Fig. 13. PV Panel output at constant condition (a) Voltage waveform (b) Current waveform.

The output characteristics of a photovoltaic (PV) panel at constant condition are demonstrated in Fig. 13. In Fig. 13(a), the voltage waveform exhibits a consistent value of 44V. However, at 0.1s, there is a slight deviation in voltage, after which it stabilizes and remains constant at 48V. Fig. 13(b) illustrates the current output of the PV panel, showing a gradual increase initially and reaching a steady state of 240A after 0.1s.

(a)

(b)
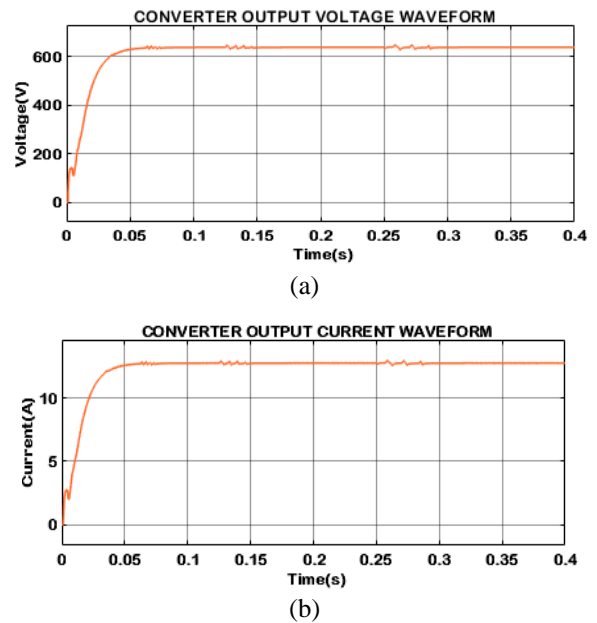
Fig. 14. Converter waveforms at constant condition (a) Voltage (b) Current.

(a)

(b)

(c)
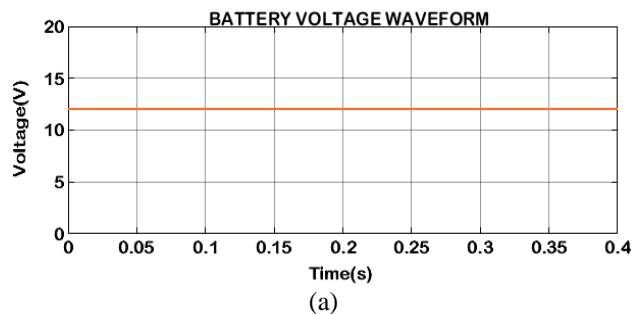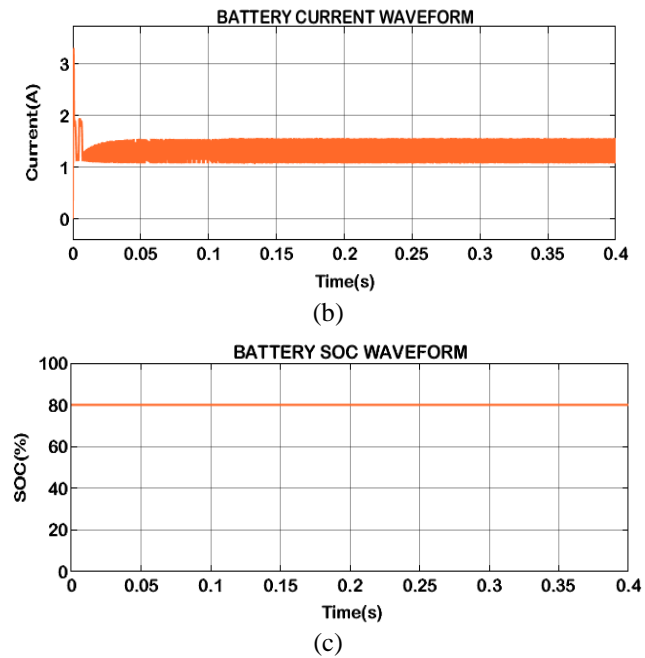
Fig. 15. Battery Waveforms (a) Voltage waveform (b) Current waveform (c) SOC waveform.

(a)

(b)
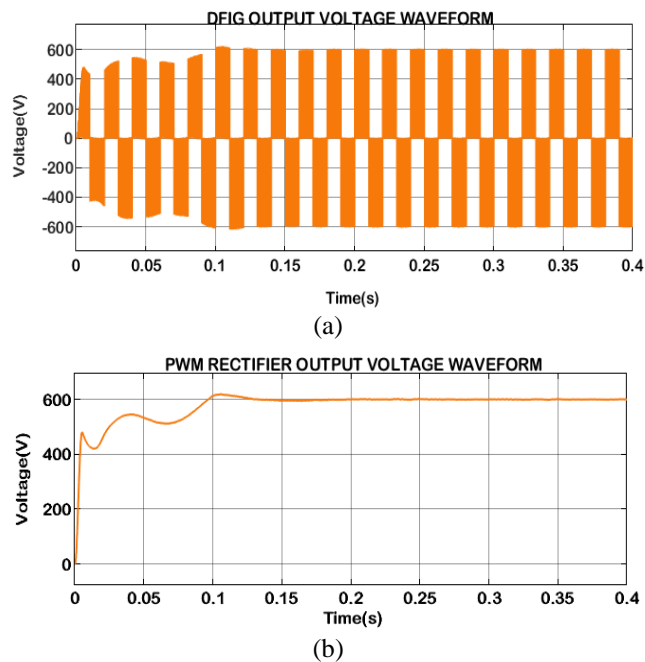
Fig. 16. Output Voltage Waveform (a) DFIG (b) PWM Rectifier.

Fig. 14 illustrates an output voltage and current waveforms generated by proposed converter, with input derived from the PV panel. In Fig. 14(a), the output voltage waveform undergoes a disturbance at 0.01s, stabilizing by 0.05s, and maintaining a constant voltage of 620V after 0.3s. Simultaneously, Fig. 14(b) portrays the converter's output current, initially experiencing a disruption and exhibiting a

gradual increase at 0.03s, followed by a constant current of 13A.

(a)

(b)

(c)

(d)
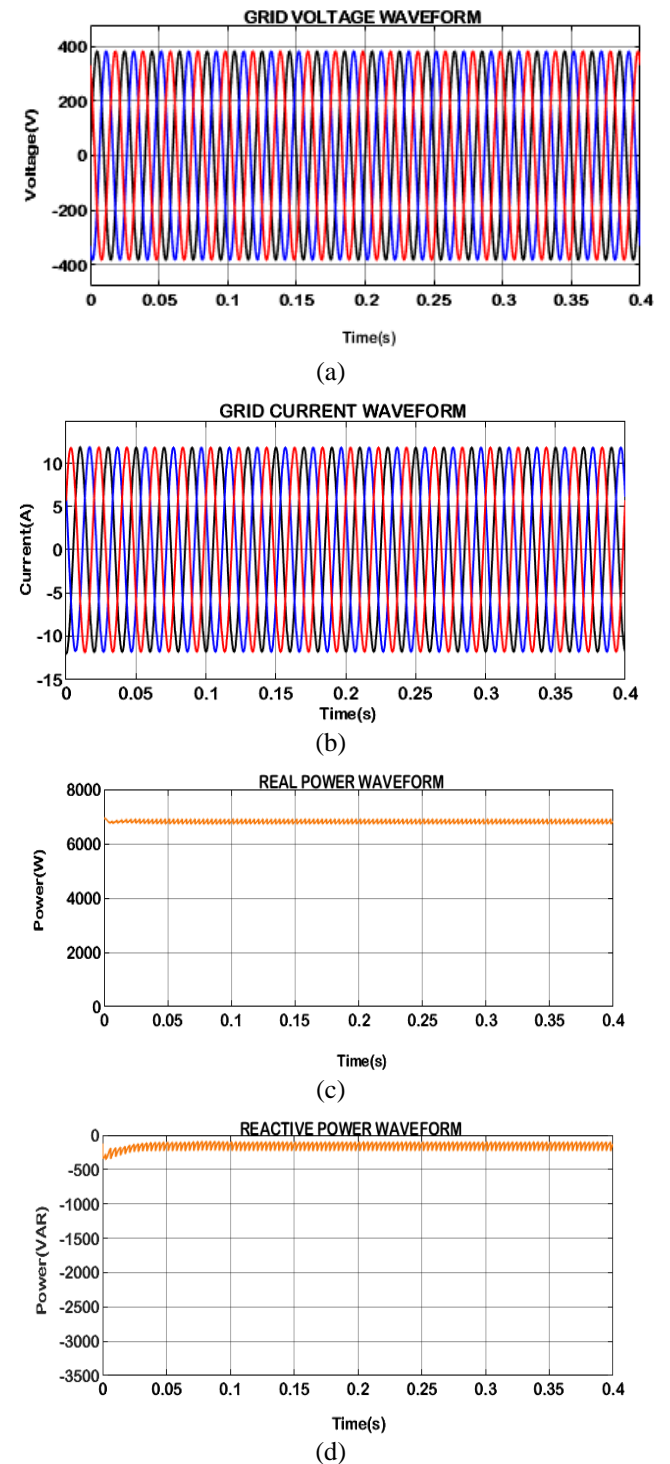
Fig. 17. Grid Waveforms (a) Voltage waveform (b) Current waveform (c) Real power (d) Reactive power.

The waveforms illustrated in Fig. 15 shows battery outputs, in which the voltage is sustained at 12V in Fig. 15(a). Similarly, the current waveform of the battery displayed in Fig. 15 (b), which is disturbed at initial stage,

and it is constantly sustained at 1.5A. Fig. 12 (c) indicates SOC of battery which is continuous to maintain at a maximum level of 80%.

DFIG and rectifier output voltage waveforms are exhibited in Fig. 16. In the first waveform displayed in Fig. 16(a), voltage is drastically raised in the beginning to 450V and there is a gradual change in the voltage and it is sustained at 600V. The second waveform in Fig. 16(b) indicates an output voltage obtained from the DFIG, in which it is initially oscillated due to the wind gust and is equally kept at 600V from 0.15s.

The waveform depiction in Fig. 17 describes an output current and voltage of grid along with reactive and real power. Initially an actual power value of 7000W is achieved, which in turn produces a constant grid voltage of about 390V with stable grid current of 12A. The real power waveform is continuously regulated at 7000W with a minimized reactive power of -200VAR.

Fig. 18 displays a graphic representation of total harmonic distortion. A grid current THD value of 2.33%, is achieved which results in lower harmonics and meets the requirement of IEEE519 standard.
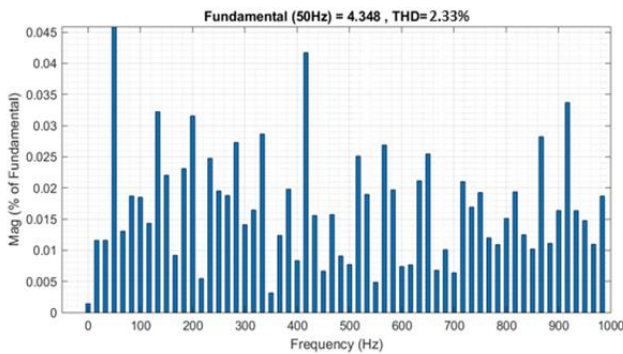
Fig. 18. THD output.

Table 3. Comparison of Settling time, Rise time And Peak overshoot

Control approach	Settling time(s)	Rise time(s)	Peak overshoot(s)
GA-PI	0.52	0.01	0.015
PSO-PI	0.44	0.011	0.010
GWO-PI	0.38	0.015	0.05
GOA-PI	0.3	0.025	0.13

Table 3 compares the peak overshot, rise time, and settling time of various optimized techniques with PI controller assistance. In contrast to other similar approaches, the proposed GOA-PI controller shows faster convergence at 0.3s. This implies that the system controlled by GOA-PI reaches a stable state more rapidly, contributing to faster convergence and improved dynamic response. This results

in a more robust and reliable control system, especially in the presence of disturbances or uncertainties.

Voltage gains and efficiency performance measures for several converters are compared in Fig. 16 and Table 4. Figure 19(a) below compares efficiency and demonstrates how the improved KY converter in the suggested system performs better than other converters. High efficiency is crucial in power conversion systems as it minimizes power losses, resulting in improved energy utilization and reduced heat dissipation.

Table 4. Comparison of voltage gain & efficiency

Converters	Voltage gain	Efficiency
Boost [30]	1.5	80%
Buck boost [34]	2	85%
Cuk [32]	3	85%
SEPIC [33]	8	88.82%
KY [31]	12.33	95%
Improved KY	13	95.2%
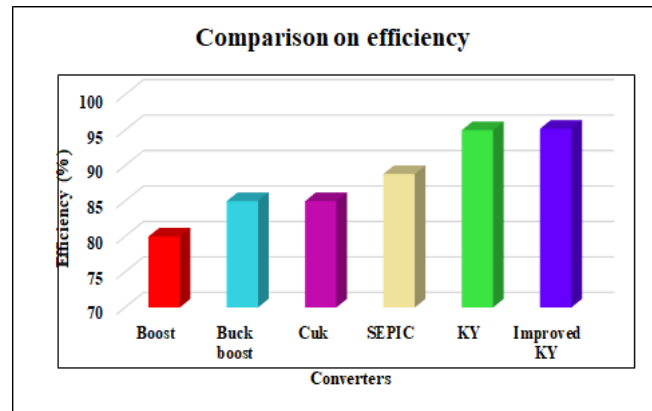
(a)
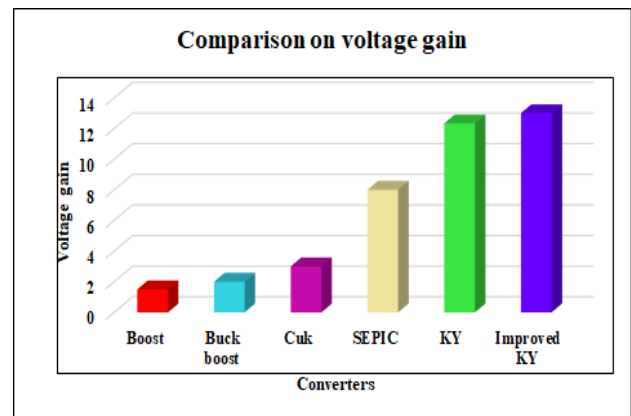
(b)

Fig. 19. Converter (a) Efficiency and (b) Voltage Gain.

On other hand, voltage gain is compared in Fig. 19 (b), for converters, in which voltage gain of 1:13 is obtained for proposed converter, which improves system performance. This higher voltage gain can be advantageous in applications where a substantial step-up in voltage is required, providing flexibility in matching different voltage levels within a system.
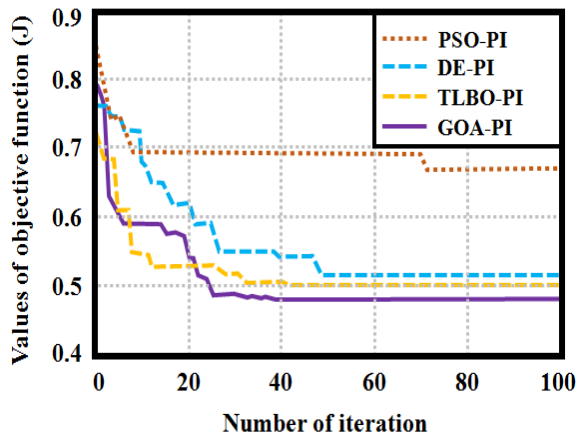
Fig. 20. Comparison of Algorithms.

The speed of the algorithms during their convergence with their maximum number of iterations appears in Fig. 20, as mentioned earlier. In the above figure, GOA based PI controller is compared with PSO-PI, GA-PI and GWO-PI, in which it is understood that GOA-PI has speed convergence rate with minimum number of iteration, which automatically increases the efficiency of the system. This implies that the control system achieves stability and optimal performance with less iteration, leading to quicker settling times and dynamic response. Fast convergence is particularly advantageous in real-time applications where rapid adjustments to changing conditions are essential.
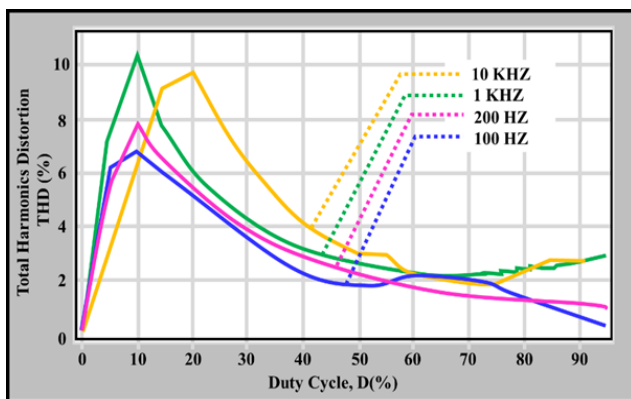
Fig. 21. Comparison of THD.

THD values at different frequencies are illustrated in Fig. 21. It denotes the level of the deformation that happens in the output waveform. THD impacts on the power system because it emerges from any variation takes place in the sinusoidal waveform, which is produced by PWM. This converter shows less harmonic distortion when compared to other configurations. By utilizing a filter across the load, THD can be suppressed even more. Low THD indicates a closer approximation to a pure sinusoidal waveform in the output. Improved waveform quality contributes to better power quality, reducing the likelihood of voltage and current distortions that can affect the performance of connected devices and equipment. Reduced harmonic distortions contribute to smoother operation, minimizing stress on components and enhancing the reliability of power electronics.

5. CONCLUSION

Recently the usage of EVs are increasing rapidly due to its reduction in the greenhouse gas emissions, improvement in the quality of air and reduces the impacts on climate conditions in urban areas and it uses electricity instead of fossil fuels like diesel and petrol. During long travel, charging of EV batteries is required and so a solar powered EV system connected to grid is designed for clean and stable charging and the EV batteries store the extra energy for future use. WECS based DFIG is preferred to attain maximum amount of wind power from the environment. In this paper, Improved KY converter is used, because it provides greater output voltage gain than its input voltage. GOA based PI controller is used because it has quick convergence speed with minimum number of iterations and has a better damping behavior. Effective grid synchronisation is accomplished using the 3ϕ VSI and PI controller with a minimum THD value of 2.33%. The proposed converter results in enhanced efficiency value of 95.2% with maximum voltage gain of 1:13 respectively.

REFERENCES

[1] Huynh, D. C.; Ho, L. D.; and Dunnigan, M. W. 2024. Modelling and Determining Parameters of a Solar Photovoltaic Cell based on Voltage and Current Measurements. GMSARN International Journal, convergence 3: 23.

[2] Lu, K.C.; Lin, F.J.; and Yang, B.H. 2017. Profit optimization-based power compensation control strategy for grid-connected PV system. IEEE Systems Journal 12(3): 2878-2881.

[3] Kavin, K.S.; and Subha Karuvelam, P. 2023. PV-based grid interactive PMBLDC electric vehicle with high gain interleaved DC-DC SEPIC Converter. IETE Journal of Research 69(7): 4791-4805.

[4] Veerachary, M.; and Kumar, P. 2020. Analysis and design of quasi-Z-source equivalent DC–DC boost converters. IEEE Transactions on Industry Applications 56(6): 6642-6656.

[5] Hasanpour, S.; Baghramian, A.; and Mojallali, H. 2019. Analysis and modeling of a new coupled-inductor buck–boost DC–DC converter for renewable energy applications. IEEE Transactions on Power Electronics 35(8):

8088-8101.

[6]   Miao, S.; and Gao, J. 2019. A family of inverting buck-boost converters with extended conversion ratios. IEEE Access 7: 130197-130205.

[7]   Anand, A.; and Singh, B. 2018. Modified dual output cuk converter-fed switched reluctance motor drive with power factor correction. IEEE Transactions on Power Electronics 34(1): 624-635.

[8]   Kushwaha, R.; and Singh, B. 2019. A power quality improved EV charger with bridgeless Cuk converter. IEEE Transactions on Industry Applications 55(5): 5190-5203.

[9]   Zhu, B.; Liu, G.; Zhang, Y.; Huang, Y.; and Hu, S. 2020. Single-switch high step-up Zeta converter based on Coat circuit. IEEE Access 9: 5166-5176.

[10] Siwakoti, Y.P.; Mostaan, A.; Abdelhakim, A.; Davari, P.; Soltani, M.N.; Khan, M.N.H.; Li, L.; and Blaabjerg, F. 2018. High-voltage gain quasi-SEPIC DC–DC converter. IEEE Journal of Emerging and Selected Topics in Power Electronics 7(2): 1243-1257.

[11] Maroti, P.K.; Padmanaban, S.; Holm-Nielsen, J.B.; Bhaskar, M.S.; Meraj, M.; and Iqbal, A. 2019. A new structure of high voltage gain SEPIC converter for renewable energy applications. Ieee Access 7: 89857-89868.

[12] Kumar, K.R.; Raja, K.R.; Padmanaban, S.; Muyeen, S.M.; and Khan, B. 2022. Comprehensive Review of KY Converter Topologies, Modulation and Control Approaches with Their Applications. IEEE Access 10: 20978-20994.

[13] Kunjittipong, N.; Kongkanjana, K.; and Khwan-on, S. 2020. Comparison of fuzzy controller and PI controller for a high step-up single switch boost converter. In 2020 3rd International Conference on Power and Energy Applications (ICPEA) (pp. 94-98).

[14] Yap, K.Y.; Beh, C.M.; and Sarimuthu, C.R. 2021. Fuzzy logic controller-based synchronverter in grid-connected solar power system with adaptive damping factor. Chinese Journal of Electrical Engineering 7(2): 37-49.

[15] Katoch, S.; Chauhan, S.S.; and Kumar, V. 2021. A review on genetic algorithm: past, present, and future. Multimedia tools and applications 80: 8091-8126.

[16] Yadav, R.K.; Hrisheekesha, P.N.; and Bhadoria, V.S. 2023. Grey wolf optimization based demand side management in solar PV integrated smart grid environment. IEEE Access 11: 11827-11839.

[17] Martinez-Rico, J.; Zulueta, E.; de Argandoña, I.R.; Fernandez-Gamiz, U.; and Armendia, M. 2020. Multi-objective optimization of production scheduling using particle swarm optimization algorithm for hybrid renewable power plants with battery energy storage system. Journal of Modern Power Systems and Clean Energy 9(2): 285-294.

[18] Zhang, Q.; and Liu, L. 2019. Whale optimization algorithm based on Lamarckian learning for global optimization problems. Ieee Access 7: 36642-36666.

[19] Meraihi, Y.; Gabis, A.B.; Mirjalili, S.; and Ramdane-Cherif, A. 2021. Grasshopper optimization algorithm: theory, variants, and applications. IEEE Access 9: 50001-50024.

[20] Ha-upala, N.; and Bhumkittipich, K. 2020. Voltage-based non-standard inverse time for over current relay in distribution system connected dfig-based wind turbines. GMSARN Int. J, 15(2): 113-120.

[21] Ewees, A.A.; Gaheen, M.A.; Yaseen, Z.M.; and Ghoniem, R.M. 2022. Grasshopper optimization algorithm with

crossover operators for feature selection and solving engineering problems. IEEE Access 10: 23304-23320.

[22] Prasad, R.M.; and Mulla, M.A. 2020. Rotor position-sensorless algorithms for direct power control of rotor-tied DFIG. IEEE Transactions on Power Electronics 36(6): 6213-6217.

[23] Moghadam, H.M.; Gheisarnejad, M.; Esfahani, Z.; and Khooban, M.H. 2020. A novel supervised control strategy for interconnected DFIG-based wind turbine systems: MiL validations. IEEE Transactions on Emerging Topics in Computational Intelligence 5(6): 962-971.

[24] Chamarthi, P.K.; Al-Durra, A.; EL-Fouly, T.H.; and Al Jaafari, K. 2021. A novel three-phase transformerless cascaded multilevel inverter topology for grid-connected solar PV applications. IEEE Transactions on Industry Applications 57(3): 2285-2297.

[25] Turksoy, O.; Ayasun, S.; Hames, Y.; and Sönmez, Ş. 2019. Computation of robust PI-based pitch controller parameters for large wind turbines. Canadian journal of electrical and computer engineering 43(1): 57-63.

[26] Liang, X.; and Andalib-Bin-Karim, C. 2018. Harmonics and mitigation techniques through advanced control in grid-connected renewable energy sources: A review. IEEE Transactions on Industry Applications 54(4): 3100-3111.

[27] Mohamed, I.S.; Rovetta, S.; Do, T.D.; Dragicević, T.; and Diab, A.A.Z. 2019. A Neural-Network-Based Model Predictive Control of Three-Phase Inverter with an Output LC Filter. IEEE Access 7:124737–124749.

[28] Hussaian Basha, C.H.; Bansal, V.; Rani, C.; Brisilla, R.M.; and Odofin, S. 2020. Development of cuckoo search MPPT algorithm for partially shaded solar PV SEPIC converter. In Soft Computing for Problem Solving: SocProS 2018, Volume 1 (pp. 727-736). Springer Singapore.

[29] Nayak, P.C.; Prusty, R.C.; and Panda, S. 2021. Grasshopper optimization algorithm optimized multistage controller for automatic generation control of a power system with FACTS devices. Protection and Control of Modern Power Systems 6: 1-15.

[30] Mosaad, M.I.; Abu-Siada, A.; and El-Naggar, M.F. 2019. Application of superconductors to improve the performance of DFIG-based WECS. IEEE Access 7: 103760-103769.

[31] Nejabatkhah, F.; Danyali, S.; Hosseini, S.H.; Sabahi, M.; and Niapour, S.M. 2011. Modeling and control of a new three-input DC–DC boost converter for hybrid PV/FC/battery power system. IEEE Transactions on power electronics 27(5): 2309-2324.

[32] Saravanan, S.; Usha Rani, P.; and Thakre, M.P. 2022. Evaluation and improvement of a transformerless high-efficiency DC–DC converter for renewable energy applications employing a fuzzy logic controller. MAPAN 37(2): 291-310.

[33] Galea, F.; Apap, M.; Spiteri Staines, C.; and Cilia, J. 2011. Design of a high efficiency wide input range isolated Cuk Dc-Dc converter for grid connected regenerative active loads.

[34] Javeed, P.; Yadav, L.K.; Kumar, P.V.; Kumar, R.; and Swaroop, S. 2021. SEPIC Converter for Low Power LED Applications. In Journal of Physics: Conference Series (Vol. 1818, No. 1, p. 012220). IOP Publishing.